PCCP

Dynamic Article Links

Cite this: *Phys. Chem. Chem. Phys.*, 2011, **13**, 2748–2757

www.rsc.org/pccp

PAPER

Hydrogen bond strength and network structure effects on hydration of non-polar molecules

R. M. Lynden-Bell,*[a] N. Giovambattista,[b] P. G. Debenedetti,[c] T. Head-Gordon[d] and P. J. Rossky[e]

Received 3rd September 2010, Accepted 11th November 2010
DOI: 10.1039/c0cp01701a

We measure the solvation free energy, $\Delta\mu^*$, for hard spheres and Lennard-Jones particles in a number of artificial liquids made from modified water models. These liquids have reduced hydrogen bond strengths or altered bond angles. By measuring $\Delta\mu^*$ for a number of state points at $P = 1$ bar and different temperatures, we obtain solvation entropies and enthalpies, which are related to the temperature dependence of the solubilities. By resolving the solvation entropy into the sum of the direct solute–solvent interaction and a term depending on the solvent reorganisation enthalpy we show that, although the hydrophobic effect in water at 300 K arises mainly from the small molecular size, its temperature dependence is anomalously low because the reorganisation enthalpy of liquid water is unusually small. We attribute this to the strong tetrahedral network which results from both the molecular geometry and the hydrogen bond strength.

1. Introduction

There is a long history of discussion of the hydrophobic effect in aqueous solutions.[1–4] One aspect of this effect is the poor solubility of gases with small, non-polar, molecules, such as methane and argon. This has been attributed variously to the strength of the hydrogen bonds between molecules, the existence of a three dimensional network in the liquid, and the small size of the water molecule. In some earlier papers[5–11] we developed modified water models with either a perturbation of the tetrahedral geometry of the water molecule or a reduction in the hydrogen bond strength. We investigated the solvation of both small hydrophobic particles and flat plates in these modified water models at 300 K and concluded that the principal reason for the low solubility in water is its small molecular size and consequent high number density.[7,8] As an important aspect of the hydrophobic effect is its temperature dependence, we now extend our studies to variable temperature and extract values of the solvation entropies and enthalpies as well as free energies.

[a] *Department of Chemistry, University of Cambridge, Lensfield Road, Cambridge CB2 1EW, UK. E-mail: rmlb@cam.ac.uk; Fax: +44 1223 336362; Tel: +44 1223 336535*
[b] *Department of Physics, Brooklyn College, CUNY, Brooklyn, New York 11210, USA*
[c] *Department of Chemical and Biological Engineering, Princeton University, Princeton, New Jersey 08544, USA*
[d] *Department of Bioengineering, University of California, Berkeley, California 94720, USA*
[e] *Institute for Computational Engineering and Sciences and Department of Chemistry & Biochemistry, University of Texas, Austin, TX 78712, USA*

Experimentally it is well known that methane, nitrogen and oxygen have a decreasing solubility in water as a function of temperature near ambient conditions, often leading to a solubility minimum. This implies that the enthalpy of the solution process is negative at low temperatures. As the enthalpy associated with the reorganisation of water molecules on dissolving a molecule from the gas phase is positive, this shows that the direct attractive interaction between the solute and water is important. In this work we use simulations to make a quantitative measurement of the contributions of the direct solvent–solute interaction and the solvent reorganisation enthalpy, and we find that the latter is larger for our model liquids with weaker hydrogen bonds. Further analysis of the thermodynamics shows that the chemical potential of the dissolved molecule has a maximum as a function of temperature implying that the process of solution from the gas phase is associated with a decrease in entropy at low temperatures. One may conclude that the hydrophobic effect is entropy-driven at low temperatures and enthalpy-driven at high temperatures.[12,13] These same non-polar gases are more soluble in organic liquids such as cyclohexane and the solubility increases with temperature. In these solvents the enthalpy change is also positive and dominates the solvation process at both high and low temperature.

Yu and Karplus[14] considered the thermodynamics of solvation in the context of integral equations. They showed that the free energies, entropies and enthalpies of solvation can each be divided into solute–solvent contributions arising from the direct interaction of the solute with the solvent, and 'cavity formation' or 'solvent reorganisation' contributions which

arise from changes in the solvent structure to accommodate the solute. They pointed out the fact that although the solvent reorganisation contributes to the total entropy and energy (or enthalpy) separately, it does not contribute to the free energy of solvation as the energy and entropy contributions cancel.

Guillot and Guissani[15] performed a pioneering study of the solubility of rare gases in liquid SPC/E water[16] along the liquid–vapour coexistence line and highlighted the magnitude of energy-entropy compensation that occurs. They concluded that the hydrogen bond network is crucial in determining the unusual solvation properties of water, but mainly in an indirect way; the network breakdown at high temperatures determines the variation in density. This provided insight as to why scaled particle theory[1,17,18] which uses experimental data on the packing fraction or density, has been so successful in predicting the solubility of hard spheres when interpolated between small and large solute sizes. For small solutes such as methane, the solubility is determined by the free volume available and thus depends on the number density of the liquid and the excluded volume of the solute, while for large solutes the probability of cavity formation is proportional to the surface area of the cavity and the surface tension (surface free energy).

This difference in the nature of hydrophobicity near large flat surfaces and around small molecules has long been recognised.[17,18] Lum, Chandler and Weeks[3,19] showed how the solvation free energy can be bridged between small and large scales. At small length scales little solvent reorganisation is needed to accommodate the small solute so that the enthalpy associated with changes in solvent structure is small, and hydrophobicity is entropically driven. By contrast, for large solutes (much greater than the size of the water molecule) solvent reorganisation is the dominant effect so that the hydrophobic effect becomes enthalpically driven. This cross-over was demonstrated in simulation by Rajamani *et al.*[21] For purely repulsive surfaces, large length-scale hydrophobicity is characterised by the formation of a nanoscale depletion layer and the disappearance of the first solvation peak in the solute–solvent radial distribution function, $g_{SL}(r)$. At small length scales, such as are discussed in this study, the first solvation shell is quite pronounced. Ben-Amotz[22] used experimental and simulation data to fit an expression for the solvation free energy of hard spheres as a function of temperature and diameter. He suggested that the point where the cavity formation entropy changes sign as a function of size provides a measure of the onset of dewetting, and found that this depends strongly on the temperature. Another approach is exemplified by the investigation by Hummer *et al.*[23] of the statistics of density fluctuations in small volumes. They found that the probability distribution of the number of molecules in a given volume is well approximated by a Gaussian distribution and showed how its second moment can be related to integrals of the liquid radial distribution function over the volume. Further research has shown that increased density fluctuations at an interface are a general and important signature of hydrophobic hydration for all length scales.[24]

Our approach is to compare the solubility in different artificial liquids formed from molecules whose intermolecular potential has been modified in a controlled way. We start from the SPC/E model due to Berendsen and colleagues[16] in which charges on the oxygen and hydrogen sites provide electrostatic forces between molecules, while Lennard-Jones interactions between oxygen sites provide an isotropic short range repulsion to balance the electrostatic attraction and hence determine the size of the molecule. In this type of model the hydrogen bonds are purely electrostatic and arise because the hydrogen sites are near the periphery of the molecule. The HOH bond angle is 109.5° which favours a local tetrahedral network. We consider two families of liquids formed by modifying the intermolecular potential. In the hybrid family, we reduce the hydrogen bond strength by changing the ratio of the electrostatic interaction to the Lennard-Jones interaction relative to the values in the SPC/E model;[16] these liquids are hybrids between pure Lennard-Jones liquids and water[6] and therefore we also use a pure Lennard-Jones liquid as a comparison. In the bent family of liquids, the molecular geometry is changed by reducing the HOH bond angle,[5] keeping the same site charges and molecular dipole moment. In these models the hydrogen bond strength increases. As all the liquids are constructed to have approximately the same number density at 300 K and 1 bar pressure, the comparison demonstrates the effect of changing the hydrogen bond strength or the molecular geometry on the network organisation of the liquids and hence solvation properties in them. In this paper we compare results for the solubility of small hard spheres and Lennard-Jones particles in these liquids. We show that, while the low solubility of small hydrophobic particles at 300 K is primarily due to the small molecular size of water and the local packing in the liquid, the unusual temperature dependence of the solubility of non-polar gases is the result of the unusually low solvent reorganisation enthalpy in water. This we attribute to both its tetrahedral network and its strong hydrogen bonds.

2. Thermodynamics of solvation

Ben-Naim[25] has clarified the discussion of solvation thermodynamics by concentrating on the change in thermodynamics when a solute molecule is moved from a fixed point in an ideal gas to a fixed point in the solvent. We use this approach as it eliminates problems concerned with different standard states and is easy to implement in simulations. Provided that the internal degrees of freedom of the solute are not changed in this process, Ben-Naim's solvation free energy ΔG^* is equal to the difference in chemical potential, $\Delta\mu^*$, of a fixed solute in the solution and in the gas phase. This is exactly the quantity determined by Widom's particle insertion method[26–28]

$$\beta\Delta\mu^* = -\ln\langle\exp(-\beta U_{SL})\rangle_0, \quad (1)$$

where U_{SL} is the interaction energy between the fixed solute molecule, S, and the solvent molecules, L, the asterix denotes a fixed solute molecule and $\beta = 1/kT$. The subscript zero denotes that the average in this equation is taken over a simulation of the neat liquid in the canonical (N,V,T) ensemble. We note that $\Delta\mu^*$ as defined above is also equal to the change in chemical potential when one solute molecule is moved from an ideal gas with number density ρ to a solution with the same number density.

Further thermodynamic properties associated with this process are found by differentiation using

$$dG = -SdT + VdP + \Sigma_i \mu_i dN_i \quad (2)$$

Thus the Ben-Naim solvation entropy and enthalpy are

$$\Delta S^* = -\left(\frac{\partial \Delta\mu^*}{\partial T}\right)_{P,N} \quad (3)$$

$$\Delta H^* = \Delta\mu^* + T\Delta S^* = \left(\frac{\partial(\beta\Delta\mu^*)}{\partial\beta}\right)_{P,N}. \quad (4)$$

These solvation quantities designated by an asterix are the differences of entropy and enthalpy between a system with a solute at a fixed point in the gas phase and a fixed point in the solution. They show the effects of coupling the solute and the solvent[25] and do not depend on standard states. They can, however, readily be related to quantities measured experimentally.[25] For example, the enthalpy of solution that would be measured by calorimetry is the difference in the partial molar enthalpies in the solution and gas phases; this is related to ΔH^* by

$$\bar{H}_\ell - \bar{H}_g = \Delta H^* - RT(1 - \alpha_P T), \quad (5)$$

where α_P is the thermal expansion coefficient of the liquid at constant pressure.

In order to evaluate these quantities a series of simulations of neat liquids were carried out in the (N,V,T) ensemble at a number of temperatures and densities corresponding to pressures near 1 bar. Widom insertion of solute particles was then used to evaluate $\Delta\mu^*$ using eqn (1). The thermodynamic derivatives which determine entropy are different when taken at constant pressure and constant volume. In this work we use the definition of ΔS^* in eqn (3) so that both ΔS^* and ΔH^* correspond to changes at constant pressure.

It is also possible to use simulation data to subdivide the entropy and enthalpy into solute–solvent and solvent–solvent contributions.[14,15] In solutions at ambient pressure the PV term is negligible so that we can equate enthalpies and energies. The enthalpy contains two terms, the direct interaction between the solute (S) and solvent (L) molecules and the change in the total interaction energy between solvent molecules on dissolving the solute. Thus we can write

$$\Delta H^* = \langle U_{SL}\rangle_0 + \Delta H_{LL} = H^*_{SL} + \Delta H_{LL}, \quad (6)$$

which defines the solute–solvent and solvent reorganisation enthalpy contributions. In the hard sphere case $U_{SL} = 0$ and $\Delta H^* = \Delta H_{LL}$ is the enthalpy change on creating the cavity at constant pressure. Yu and Karplus[14] showed that $\Delta\mu^*$ is purely a solute–solvent term and has no solvent–solvent contribution. If we follow their argument, then, using $S = (H - G)/T$ for solute–solvent and solvent reorganization terms separately, we obtain

$$S^*_{SL} = (H^*_{SL} - \Delta\mu^*)/T \quad (7)$$

and

$$\Delta S^*_{LL} = \Delta H_{LL}/T \quad (8)$$

so that

$$\Delta S^* = S^*_{SL} + \Delta H_{LL}/T. \quad (9)$$

Thus we can write the solvation free energy as

$$\Delta G^* = \Delta\mu^* = H^*_{SL} - TS^*_{SL}. \quad (10)$$

as an alternative to

$$\Delta G^* = \Delta\mu^* = \Delta H^* - T\Delta S^*. \quad (11)$$

One remarkable result of the division in eqn (10) is that one can argue[15,29,30] that the driving force for hydrophobicity is purely a solute–solvent effect. However we shall see that the solvent reorganisation enthalpy plays an important role in the temperature dependence of solubility.

Laziridis[4,31–33] uses a different separation of the solvation entropy into solvent–solvent and solute–solvent terms. He calculates the entropy directly from angle dependent radial distribution functions of water molecules around a solute and water molecules around other water molecules. Neglecting the contribution of three particle and higher correlations to the entropy he obtains expressions for S^*_{SL} and ΔS^*_{LL} which can be evaluated. The advantage of this method is that contributions from different regions can be compared; the disadvantage is that computations are expensive and approximations to three particle and higher correlations have to be made.

Experimentally gas phase solubilities are measured by either the Ostwald solubility, K_{ost} or by the Henry's Law constant K_{hen}. The Ostwald solubility is just the ratio of the number density of solute molecules in the solution phase ρ_ℓ to that in the gas phase ρ_g

$$K_{\mathrm{ost}} = \left(\frac{\rho_\ell}{\rho_g}\right)^{\mathrm{eq}}, \quad (12)$$

while Henry's constant is the ratio of the partial pressure of the solute in the gas phase to the number density in the solution phase

$$K_{\mathrm{hen}} = \left(\frac{P_g}{\rho_\ell}\right)^{\mathrm{eq}} = (fRT)K^{-1}_{\mathrm{ost}} \quad (13)$$

where f is a constant relating the units used for pressure to those used for ρRT and we have assumed ideal gas behaviour. Another measure of solubility is the ratio of the partial pressure to the mole fraction, x, of solute in solution, which in dilute solution is given by

$$K_x = \left(\frac{P_g}{x}\right)^{\mathrm{eq}} = (f\rho_W RT)K^{-1}_{\mathrm{ost}}, \quad (14)$$

where ρ_W is the number density of the solvent. If the gas can be treated as ideal, K_{ost} is directly related to the solvation chemical potential by

$$\ln K_{\mathrm{ost}} = -\Delta\mu^*/RT. \quad (15)$$

The temperature derivative of the Ostwald solubility is determined by eqn (4)

$$\frac{\mathrm{d}\ln(K_{\mathrm{ost}})}{\mathrm{d}T} = \frac{\Delta H^*}{RT^2}. \quad (16)$$

which depends on both the solvent–solute enthalpy and the solvent reorganisation enthalpy. The temperature dependence of Henry's constant and the mole fraction solubility are

$$-\frac{\mathrm{d}\ln(K_{\mathrm{hen}})}{\mathrm{d}T}=\frac{\Delta H^{*}-RT}{RT^{2}}$$
$$-\frac{\mathrm{d}\ln(K_{x})}{\mathrm{d}T}=\frac{\Delta H^{*}-RT(1-\alpha_{P}T)}{RT^{2}}. \quad (17)$$

Although all three measures of solubility have different temperature dependences, we shall see the differences are small.

3. Models

Our modified water models are based on the intermolecular potential for the SPC/E model which is the sum of pair terms:

$$U(r)=4\varepsilon\left[\left(\frac{\sigma}{r_{ij}}\right)^{12}-\left(\frac{\sigma}{r_{ij}}\right)^{6}\right]+\sum_{H,O}\frac{1}{4\pi\varepsilon_{0}}\frac{q_{\alpha}q_{\beta}}{r_{\alpha\beta}}, \quad (18)$$

with the Lennard-Jones interaction centred on the oxygen sites, i and j, of a pair of water molecules, and the Coulomb interaction evaluated over all pairs of atomic sites on different molecules. The charges are −0.8476 e on the oxygen site and +0.4238 e on the hydrogen site. The value of ε is 0.6502 kJ mol^{-1} and that of σ is 0.3166 nm.[16] The rigid molecular geometry of SPC/E has bond lengths of b = 0.1nm and an HOH bond angle of 109.5°.

In the first family, the hybrid family, the Lennard-Jones interaction is increased by multiplying the value of the Lennard-Jones ε by a factor of λ. As a result the hydrogen bond weakens due to an increase in equilibrium molecular separation; the charges are kept constant.

The values of λ used in this work are λ = 1.5 for the weakly modified H15 liquid and λ = 3.0 for the strongly modified H30 liquid. Table 1 gives the relative hydrogen bond strengths, as measured by the electrostatic energy of the dimers, which are reduced by factors of 0.86 and 0.69 respectively. We also used a reference Lennard-Jones liquid (LJ3) with ε_{LJ} = 3 kJ mol^{-1}, σ = 2.876 Å, which has approximately the same number density as water at 300 K and 1 bar. In the bent family of models, the bond angle is reduced from tetrahedral, keeping the charges and molecular dipole moments constant. In this work, as in most of our earlier papers,[5,7,8,10] the Lennard-Jones σ was adjusted to give a density of approximately 1 g cm^{-3} at 300 K and 1 bar. In this paper we consider the weakly modified model, B105 with a bond angle of 105°, and the strongly modified liquid, B90, with bond angle of 90°. Table 1 lists the potential parameters and relative hydrogen bond strengths as determined from dimer energies. The hydrogen bond strengths in the bent family are *increased* by factors of 1.04 (B105) and 1.39 (B90).

Table 1 Modified water models: potential parameters and relative hydrogen bond strengths

Model	Angle/deg	b/Å	ε/kJ mol^{-1}	σ/Å	H bond strength
SPC/E	109.47	1.0	0.6502	3.166	1.00
H15	109.47	1.0	0.9753	3.166	0.86
H30	109.47	1.0	1.9506	3.166	0.69
LJ3			3.0	2.876	0.0
B105	105	0.948	0.6502	3.14	1.04
B90	90	0.816	0.6502	3.06	1.39

Table 2 summarises some properties of these liquids. The hybrid liquids span the range between tetrahedral liquids and normal organic liquids as exemplified by a Lennard-Jones liquid. Their properties show the effects of decreasing the hydrogen bond strength while keeping the preference for tetrahedral coordination. The liquids all have approximately the same number density at 300 K and 1 bar. In our earlier work[6,11] we found that the oxygen–oxygen radial distribution function $g_{LL}(r)$ changes dramatically in this family, particularly in the position of the second peak and the number of neighbours in the first shell. In SPC/E water the first peak in the radial distribution function is narrow and the ratio of the distances of the second and first peaks is about 1.6. In the H15 liquid the second peak is almost non-existent, while in the H30 liquid $g_{LL}(r)$ is very similar to the Lennard-Jones liquid LJ3 with a pronounced second peak at about twice the distance of the first peak. The number of first shell neighbours, N_n, increases from about 4.5 for SPC/E water to about 12.6 for both the H30 liquid and the LJ3 liquid. From the point of view of the structure the H30 liquid seems very similar to the Lennard-Jones liquid, although the numbers in Table 2 show that the binding energy and the critical temperatures of the H30 liquid are much higher than those of the LJ3 liquid. The tetrahedral order parameter,[34] q, decreases as the potential is modified, demonstrating the reduction in the tetrahedral network structure as the hydrogen bonds are weakened.

In the bent family of models, by contrast, individual hydrogen bond strengths increase as the bond angle is reduced, but, as the three dimensional tetrahedral network becomes less possible with the altered geometry, q decreases, and the total binding energy decreases. Model B105 still has a significant local tetrahedral network at 300 K with a tetrahedral order parameter only reduced to 0.57, the ratio of second to first peak positions still at the tetrahedral value of 1.6, and only a small increase in number of nearest neighbours. In model B90 there is little evidence of network structure. Unlike the hybrid family, the critical temperatures are found to decrease in the bent family.

Thus the hybrid family shows the effect of reducing the local network structure by reducing the hydrogen bond strength, while the bent family shows the effects of reducing the local network structure by changing the molecular geometry.

4. Simulations

Simulations were carried out using a modified version of DL_POLY.[35] In each simulation 600 molecules of one of the model liquids were placed in a dodecahedral box with fcc periodic boundaries. The distance between a molecule and its nearest image depends on the temperature, but is in the range 29–32 Å except at the highest temperatures. A run at the desired temperature was performed under conditions of constant pressure, and then the box size adjusted to the average box size in this constant pressure run. A short constant volume run was performed for further equilibration, followed by a longer production run during which configurations were saved to a trajectory file every picosecond. The long range

Table 2 Properties of liquids made from modified water models at 300 K

Model	U[a]	U_{elec}[a]	q[b]	r_2/r_1[c]	N_n	T_c[d]
SPC/E	–46.3	–55.3	0.63	1.6	4.5 ± 0.2	640
H15	–41.6	–45.6	0.56	(2.4)	9 ± 0.8	630
H30	–41.7	–34.9	0.49	2.0	12.7 ± 0.2	678
LJ3	–16.8	0	0.38	1.9	12.6 ± 0.2	475
B105	–40.7	–46.9	0.57	1.6	5.8 ± 0.4	
B90	–33.2	–35.8	0.46	1.9	10.2 ± 0.3	508

[a] Configurational energies (total and electrostatic) in kJ mol^{-1}. [b] Tetrahedral order parameter.[34] [c] Ratio of positions of second and first peaks in $g_{OO}(r)$. [d] Critical temperature in K from ref. 10.

electrostatics were treated by the Ewald summation method, and a correction was applied for the long range Lennard-Jones energies based on a continuum approximation. The time step used was 2 fs; the cutoff for the Lennard-Jones and the real space part of the Ewald sum was set to 12 Å; the temperature was controlled by a Berendsen thermostat with relaxation time 0.1 ps; the Ewald sum was evaluated with a precision of 10^{-5}; the equations of motion of rigid molecules were integrated using a quaternion algorithm.

In order to compare results for inserted Lennard-Jones particles and hard spheres one needs to determine the equivalent hard sphere diameter corresponding to a particular value of σ_{SL} between the inserted particle and the water oxygen site. This was done from the radial distribution functions, g_{SL} of a 3 Å Lennard-Jones solute in the water models. The position of the first peak was remarkably constant in all model liquids at 300 K and its position did not change with temperature. The value for the distance of closest approach of an equivalent hard sphere solute to an oxygen atom was taken from the steep part of the initial rise of the first peak in g_{SL} and determined to be 2.82 Å. This is the exclusion radius, R_{SL}, determining the size of cavity containing no oxygen sites. The exclusion radius is equal to the sum of the radius of the inserted hard sphere and the effective hard sphere radius of a water molecule which, determined from the water–water $g_{LL}(r)$ in the same way, is 1.3 Å.

The chemical potentials of both types of particle were determined from the stored trajectories from the neat liquids. A grid of 24×10^4 points separated by approximately half an Ångstrom was used for each configuration. Attempted insertions of Lennard-Jones particles with $\varepsilon_{SS} = 0.6502$ and various sizes from $\sigma_{SL} = 1$ Å to 4.5 Å were made, and the chemical potentials, $\Delta\mu^*$, calculated from eqn (1). In the modified liquids the value of ε_{SL} was determined from the Lorentz Berthelot rules. The hard sphere chemical potentials $\Delta\mu^*(R)$ were determined from the cavity distribution function $p_{cav}(r)$ by finding the radius r of the largest spherical cavity that could be centred on each grid point and using the expression

$$\frac{\Delta\mu^*(R)}{RT} = -\ln\left(\int_R^\infty p_{cav}(r)\mathrm{d}r\right). \qquad (19)$$

The curves of $\Delta\mu^*(T)$ were fitted by quadratic or cubic functions of the temperature, so that the solvation entropies could be determined from the derivative as given in eqn (3). Good fits could be found for all the modified water models, but the LJ3 liquid gave only satisfactory fits. Once the solvation entropies and chemical potentials were found, the enthalpies were determined from eqn (4) and the division into solute–solvent and solvent–solvent terms made using eqn (6) and (9).

4.1 Precision and accuracy

The precision of the results for the chemical potentials of the inserted particles, whether Lennard-Jones or hard spheres, can be estimated either by treating the results from different configurations as independent or by plotting the value as a

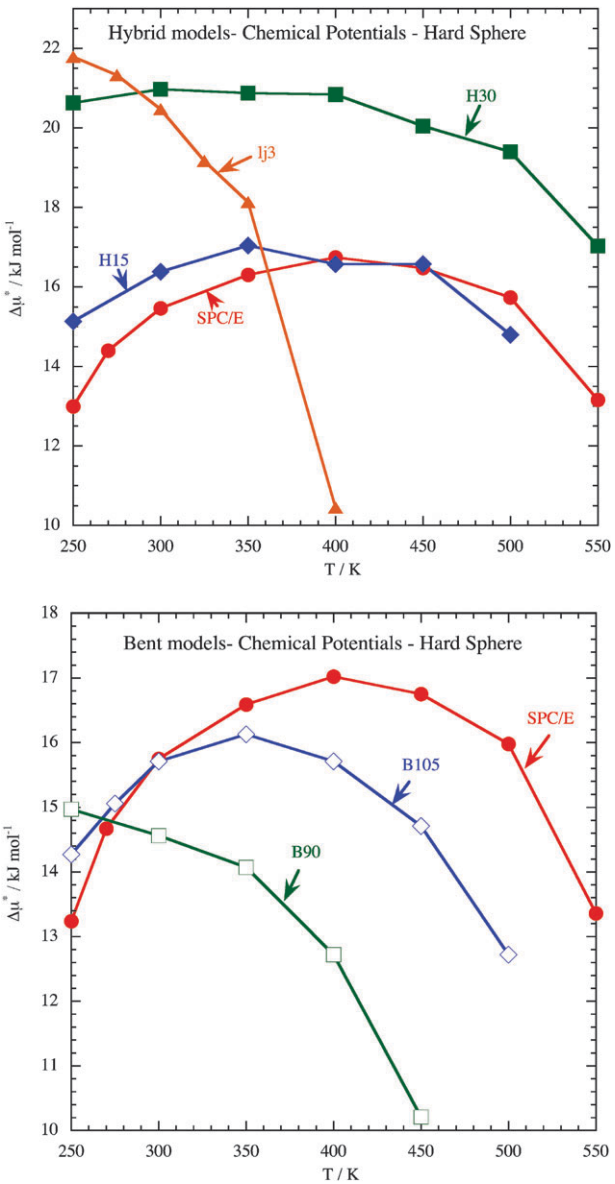

Fig. 1 Chemical Potentials of dissolved hard spheres with exclusion radius $R_{SL} = 2.82$ Å in various liquids. Above: hybrid models; below: bent models. Note that decreasing the hydrogen bond strength, while keeping the molecular geometry unchanged (hybrid models), increases the solvation chemical potential, but destroying the molecular structure geometry while leaving unchanged the site partial charges (bent models) decreases it.

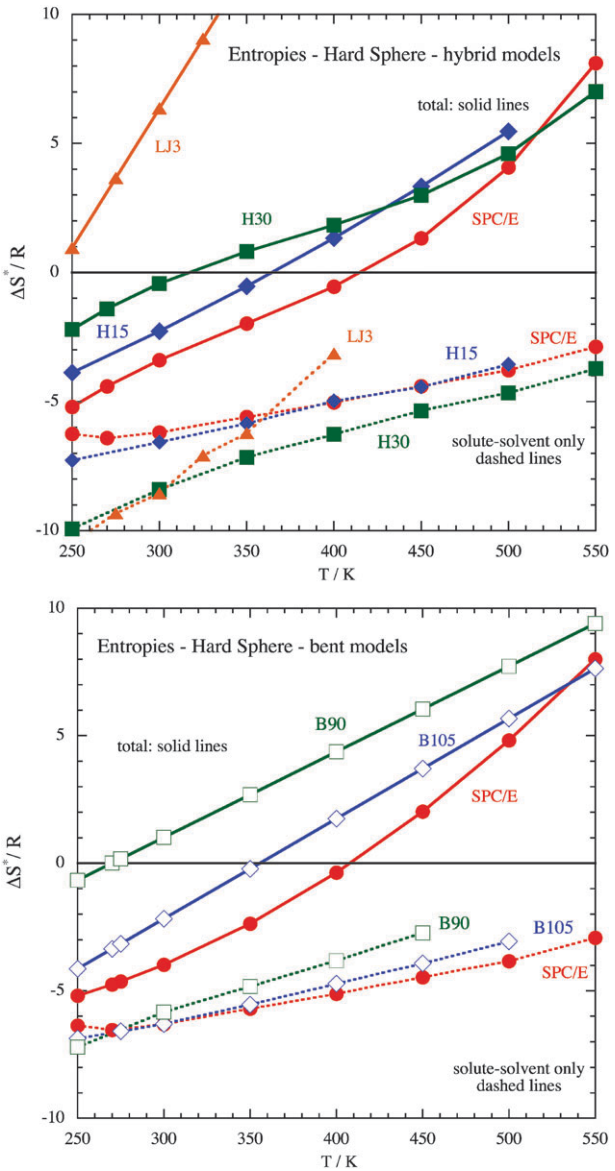

Fig. 2 Solvation entropies of hard spheres with R_{SL} = 2.82 Å in various liquids as a function of temperature. Symbols connected by full lines show the total solvation entropies while symbols connected by dashed lines show the solvent–solute contributions. Note that either reducing the hydrogen bond strength (hybrid models) or changing the molecular geometry (bent models) increases the total solvation entropy.

function of number of configurations processed. Either method gives a high precision (better than 1%) for the chemical potentials provided that the insertion probability is reasonably high, for example for hard sphere insertions with $\Delta\mu/RT < 15$ or Lennard-Jones insertions with $\Delta\mu/RT < 6$.

However Fig. 1 for the chemical potentials as a function of temperature shows deviations from smooth curves. The principal reason for the discrepancy seems to be difficulty in obtaining the precise density corresponding to the required temperature and one atmosphere pressure. An estimate of the error can be made by comparing the results from NVT simulations of the LJ3 liquid at state points with T = 300 K and density 0.986 g ml^{-1} which had P = 0.003 kbar and with T = 300 K and density 1 g ml^{-1} which had a pressure of 0.986 kbar. The hard sphere chemical potential at these two state points was 8.55RT and 8.21RT respectively. This suggests that the errors in the chemical potentials are about ±0.4 kJ mol^{-1}, which are acceptable in the present context.

As the solvation entropies depend on the fitting of the chemical potential curves to a polynomial function, their errors are likely to be larger, ranging from 0.5R to about 1R at the highest and lowest temperatures considered, respectively. In the LJ3 liquid where the fitting was less satisfactory, the errors are probably greater. It should also be noted that at the lowest temperature considered most of the liquids had somewhat sluggish dynamics, and even though the runs were typically twice as long, errors are expected to be somewhat larger at these lowest temperatures.

5. Results and discussion

We start by discussing the results for hard sphere solutes. We then consider and compare the results for Lennard-Jones spheres, which, although less hydrophobic, are more realistic representations of small molecules.

Fig. 1 shows the variation of the solvation chemical potential of hard spheres with an exclusion radius of 2.82 Å in different liquids as a function of temperature at or near one atmosphere pressure. The upper panel compares SPC/E water with the weakly modified hybrid model H15 and the more strongly modified hybrid model H30 with progressively decreasing hydrogen bond strengths. In each of these liquids there is a broad maximum which is at about 400 K for SPC/E water, but moves to lower temperatures as the liquid becomes more Lennard-Jones like. The pure Lennard-Jones LJ3 liquid does not show a maximum in the accessible temperature range. The temperature dependence of the solvation chemical potentials is primarily the result of changes in density. As the solvation entropy, ΔS^*, is equal to minus the slope of the graphs of $\Delta\mu^*$ (eqn (3)) the presence of a maximum chemical potential shows that for the liquids SPC/E, H15 and H30 the solvation entropy is negative at low temperatures and positive at high temperatures, but it is always positive for the Lennard-Jones liquid. The lower part of the figure shows the results for bent liquids, which have progressively reduced bond angles. The main contrast of these liquids with the hybrid ones is that changing the geometry reduces the solvation chemical potential, while reducing the hydrogen bond strength increases it. Thus for this property the behaviour of water is not extreme. In our earlier work at 300 K[7] we related the solvation chemical potential to the width of the cavity distribution function. We found that the hybrid liquids have narrower distributions as they are more close packed. The bent models, on the other hand, have broader distributions at ambient conditions.

The changes with temperature are closely related to changes in density, that is to the coefficient of thermal expansion, $\alpha_P = (\partial lnV/\partial T)_P$. Of the liquids considered here, SPC/E has an abnormally low coefficient of thermal expansion at 300 K $\alpha_P = 0.5 \times 10^{-3}$ K^{-1} [36] (in real water it is even lower, 0.25×10^{-3} K^{-1}). Model liquids H15, H30 and B105 have somewhat larger values of $\alpha_P = 0.8 - 0.9 \times 10^{-3}$ K^{-1},

while the liquid B90 with no three dimensional network has $\alpha_P = 1.5 \times 10^{-3}$ K^{-1} which is comparable to the values found for non-associated liquids ($1.2 - 1.6 \times 10^{-3}$ K^{-1}) such as carbon tetrachloride and acetone.

Fig. 2 shows the total solvation entropy (full lines) as a function of temperature for hybrid liquids (above) and bent liquids (below). In addition, the solute–solvent part of the entropy as defined in eqn (9) is shown by dotted lines. The latter is always negative, because the average probability of insertion of a hard sphere is always less than one; it also increases (becomes less negative) as the temperature increases. The 'typically aqueous'[37] change of sign of the total entropy and hence the maximum in the chemical potentials arises from a change in the balance between the solute–solvent entropy S_{SL} and the solvent reorganisation entropy $\Delta S_{LL} = \Delta H_{LL}/T$ defined in eqn (9). Further, considering both families, the total solvation entropy is least in SPC/E water, with the change in sign occurring at the highest temperature. Thus for this property, SPC/E water shows extreme behaviour. Comparing the total and solute–solvent contributions one sees that this striking result can be traced to the variation in solvent reorganisation enthalpies.

These are shown in Fig. 3 for hard sphere solutes for which the total solvation enthalpy and the solvent reorganisation enthalpy are equal, $\Delta H_{LL} = \Delta H^*$. It is the fact that the solvent reorganisation enthalpies increase with temperature that causes the change of sign of the total solvation entropy, and the fact that the solvent reorganisation enthalpy is lower in SPC/E water than in any of the modified water models that causes the temperature of this change of sign to be highest in this liquid. Unlike the solvation chemical potential, the solvation entropy and enthalpy are lower in SPC/E water than in any of the modified water models. Water's behaviour in this context is extreme.

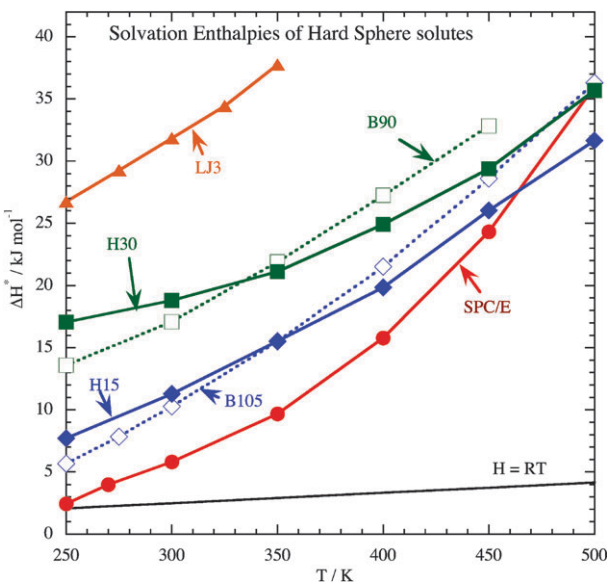

Fig. 3 Solvation enthalpies for hard spheres with $R_{SL} = 2.82$ Å in various liquids. Bent models are distinguished by open symbols and dotted lines. Note that ΔH^* is least in SPC/E water. It increases with temperature and is greater than RT in all these liquids above 250 K.

The results for the dissolved Lennard-Jones solutes with $\sigma_{SL} = 3$ Å are closely related to those presented for hard sphere solutes. We illustrate this with results from the hybrid H30 liquid as an example. Comparable similarities and differences between hard sphere and Lennard-Jones solutes are obtained for the other liquids. Fig. 4 shows the total entropies (solid lines) and the solute–solvent entropies (dotted lines) for hard sphere and Lennard-Jones spheres of the same effective size in the hybrid H30 liquid. The difference between the solutes is remarkably small. Similar results were found in the other liquids, suggesting that solvation entropies mainly arise during the formation of a cavity to contain the solute. Fig. 5 shows contributions to the solvation enthalpy for the two types of solute in H30 liquid. The solvation enthalpy, ΔH^*, for the Lennard-Jones sphere (solid red curve) is lower than for the hard sphere (green curve) because of the direct solvent–solute interaction, U_{SL}, (blue curve), but the solvent-reorganisation enthalpy change on insertion of the Lennard-Jones sphere (red dotted curve) is only slightly less than the change on insertion of a hard sphere (green curve).

Fig. 6 shows that there is a progression of solvation enthalpies of Lennard-Jones spheres in the modified liquids, which is similar to that observed for hard sphere solutes (see Fig. 3). In all the liquids ΔH^* for a Lennard-Jones solute increases with temperature and is least in SPC/E water. The significant difference between Lennard-Jones and hard sphere solutes of this size is that in liquids SPC/E, and the slightly modified liquids B105 and H15, the Lennard-Jones solvation enthalpies are negative at low temperatures while the hard sphere solvation enthalpies are always positive. In the strongly modified liquids B90 and H30 the solvation enthalpies are always positive. As the Ostwald solubility as a function of temperature is a minimum when $\Delta H^* = 0$, this figure shows that the temperature of minimum Ostwald solubility is reduced for the slightly modified liquids B105 and H15, while the Ostwald solubility of Lennard-Jones particles with $\sigma = 3$ Å always increases with temperature in the more strongly modified liquids, B90 and H30. We note that if either of the other measures of solubility are used, then the conditions for the change of sign is that either $\Delta H^* - RT$ (Henry's Law) or $\Delta H^* - RT(1 - \alpha_P T)$ (mole fraction) change sign as a the temperature is raised. However RT is small, being equal to 2.5 kJ mol^{-1} at 300 K and 4.6 kJ mol^{-1} at 550 K and, as shown in Fig. 6, is small compared to the changes in ΔH^*. The factor $RT(1 - \alpha_P T)$ is even smaller, so that the temperatures of minimum solubility as measured by Henry's Law or by the mole fraction are somewhat higher than the corresponding temperature for the Ostwald solubility, but the qualitative behaviour is the same.

6. So what really causes hydrophobicity on short length scales?

The principal experimental manifestation of the hydrophobic effect on short length scales is the low solubility of non-polar gases in water at ambient conditions. The thermodynamic reason for this is a high positive value of the solvation chemical potential, $\Delta\mu^*$. The chemical potential is determined by the balance between the difficulty of finding a cavity of the

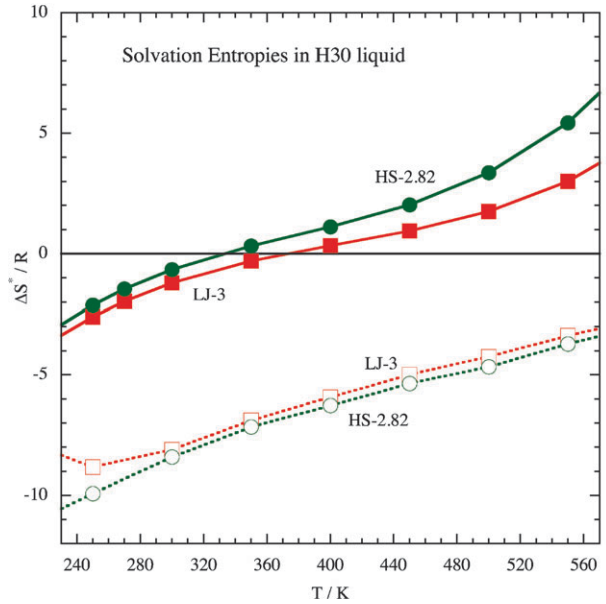

Fig. 4 Contributions to solute entropies in liquid H30 at 300 K. The circular and square symbols connected by solid lines are the total solvation entropies for hard spheres with R_{SL} = 2.82 Å and Lennard-Jones spheres with σ_{SL} = 3 Å respectively. Symbols connected by dotted lines are the corresponding solute–solvent contributions.

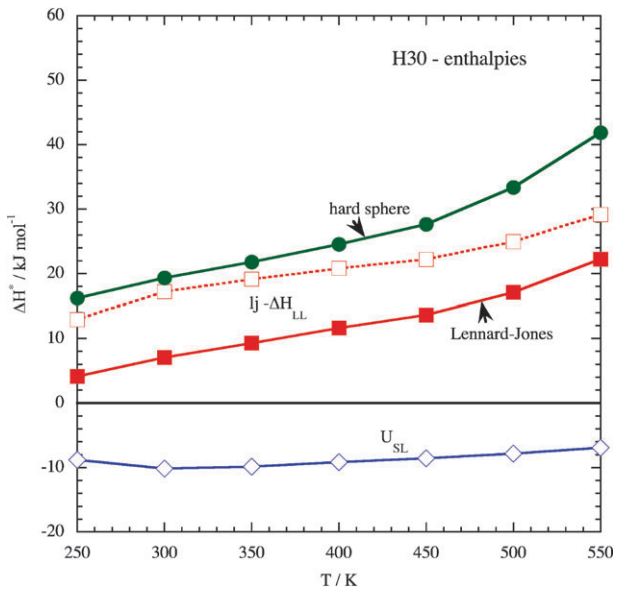

Fig. 5 Contributions to solvation enthalpies in liquid H30 at 300 K. The square symbols connected by solid lines show the total solvation enthalpy while the open symbols connected by dotted lines show the reorganisation enthalpy for Lennard-Jones spheres with σ_{SL} = 3 Å. U_{SL} (diamond symbols) is the direct solute–solvent interaction energy for the Lennard-Jones solute. The circular symbols show the reorganisation enthalpy (equal to the total enthalpy) for the same sized hard sphere. Note that the solvent reorganisation enthalpies are similar.

correct size to contain the solute ($-TS^*_{SL}$) and the solute–solvent attraction (U_{SL}), if any.[24] In water the latter term does not overcome the entropic term for non-polar solutes, and in this sense we can say that the hydrophobic effect is entropy-driven specifically by the solute–solvent entropy.

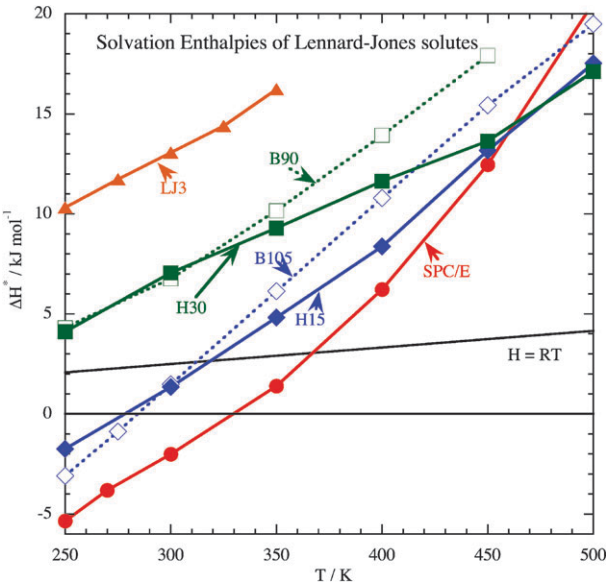

Fig. 6 Solvation enthalpies of 3 Å Lennard-Jones spheres in various liquids as a function of temperature. Bent models are distinguished by open symbols and dotted lines. Note that the solvation enthalpy is lower in the SPC/E water compared to liquids from either family, and that H^* in SPC/E water crosses the $H = RT$ line at a higher temperature than the weakly modified models H15 and B105, while in the more strongly modified models H30 and B90 and the Lennard-Jones liquid LJ3, H^* does not cross this line.

In our series of liquids we find that the negative values of S^*_{SL} arise, as suggested by previous workers,[12,15] from the dense packing of the water which restricts the size of the cavities. This is not a peculiarity of water, as our artificial liquids in the hybrid family have higher values of $\Delta\mu^*$ than SPC/E water at ambient conditions. These liquids have the same number density, but have a more nearly close packed liquid structure, which results in narrower cavity distribution functions with the same peak position. One can also correlate the width of the cavity distribution function with the density fluctuations in the liquid.[23] In our earlier work[7,9] we found that bent models with smaller bond angles had broader cavity distribution functions than SPC/E water and so were more able to dissolve small solutes. We concluded that the low solubility of hard spheres at 300 K depends strongly on the local packing, but not directly on the existence of a local tetrahedral network. The role of hydrogen bonding is indirect, as without strong intermolecular interactions water would not be a liquid at ambient conditions. In organic solvents the molecules are bigger and the dispersion interactions are larger, so that $-TS^*_{SL}$ and U_{SL} are both smaller (more negative), reducing the solvation chemical potentials. Although several authors[1,3,12] support this view, the importance of solvent cohesive energy has been highlighted by others.[4]

Another observed characteristic of hydrophobic hydration for small molecules is that the molecular solubility decreases with temperature at ambient conditions, but increases at higher temperatures. We have seen from eqn (4) that if this is true for the Ostwald solubility, the solvation enthalpy, ΔH^*, is negative at ambient conditions, but changes sign at higher temperatures. ΔH^* is the balance between a negative

contribution from the direct solute–solvent interaction and the positive contribution from the solvent reorganisation energy, which increase with temperature. Although this property is often invoked as a characteristic of hydrophobic hydration, it is clear that it does not apply to hard spheres, the ultimate hydrophobic solutes. This distinction in behaviour between hard spheres and attractive solutes, resulting from the direct interaction term, has sometimes not been highlighted.[38] We find from the present simulations that the difference between water and the hybrid models is one of degree, but the increasing solvent reorganisation energy in successive members of the hybrid family (see Fig. 6) means that Lennard-Jones spheres with the parameters studied here have decreasing solubility at low temperature in only SPC/E water and the intermediately modified liquids H15 and B105. We conclude that the anomalous temperature dependence of the hydrophobic effect is due to the abnormally low solvent reorganisation energy in water which in turn is due to the strong three dimensional network structure. Another manifestation of the network structure is in the coefficients of thermal expansion, α_P. This is particularly low for SPC/E water at 300 K, slightly higher for model liquids H15, H30 and B105 and twice as large for liquids B90 with no three dimensional network.

It is often stated that the hydrophobic effect changes from being entropy driven to enthalpy driven as the temperature increases. Fig. 4 shows how the total solvation entropy ΔS^* changes sign as the temperature increases, even though the solute–solvent term S^*_{SL} is always negative (albeit increasing). Remembering that (see eqn (9)) $\Delta S^* = S^*_{SL} + \Delta H_{LL}/T$, this result confirms the importance of the contribution of the solvent reorganisation energy to the temperature dependence of the chemical potential $\Delta\mu^*$ as well as to the change in solubility with temperature.

A useful approach to the analysis of solvation which is often invoked is to consider the process as occurring in two steps, firstly the formation of a cavity and secondly the change in thermodynamics due to the interaction of the solute with the surrounding solvent. In this study we have found that for small solutes the solvation entropy and the solvent reorganisation enthalpy arise in the first of these processes while the total solvation enthalpy and hence the chemical potential depend on both steps. These observations support the use of a first order perturbation approach such as that used by Ben-Amotz.[22,39]

Graziano[40] investigated the solubility of hard spheres in several liquids as a function of the size of the cavities using scaled particle theory and experimental values for the packing fraction, number density and coefficient of thermal expansion of each solvent. The scaled particle expressions are

$$\Delta G^*_{\mathrm{cav}} = RT \times g(\xi, (\sigma_c/\sigma)) \qquad (20)$$

$$\Delta H^*_{\mathrm{cav}} = -\alpha_P RT^2 \times h(\xi, (\sigma_c/\sigma)) \qquad (21)$$

where g and h are functions of the packing fraction, ξ, of the neat liquid and the ratio σ_c/σ of the cavity diameter to the molecular diameter. The solvation thermodynamics of hard spheres (or cavities) in water at ambient conditions shows that, according to scaled particle theory, ΔG^* is dominated by the $T\Delta S^*$ term with a comparatively small value of ΔH^*, while in alcohols (ethanol and methanol) and non-polar liquids (benzene, cyclohexane and carbon tetrachloride) the $T\Delta S^*$ term is less negative and the solvent reorganisation term ΔH_{LL} is larger. Eqn (21) shows that, at least within the scaled particle theory, the reason for the small value of the solvent reorganisation enthalpy in water is its small value of the coefficient of thermal expansion, α_P. ΔS^* is large and negative because its molecular size σ is small. We note that in this theory $\Delta G^*/T$ only depends on the packing fraction and the molecular size; the role of hydrogen bonds is indirect in that the strong intermolecular forces allow the material to be in the liquid state rather than a gas.

Pratt, Chandler and coworkers[3,19,20,23] have pursued the idea of information theory in the context of hydrophobic hydration. They find that the probability distribution of the number of solvent molecules in a volume v is approximately Gaussian. The solvation free energy of a hard sphere depends on the logarithm of the probability of finding that the corresponding volume v is empty. Assuming that the probability distribution is Gaussian, one can write

$$\Delta\mu^*/k_{\mathrm{B}}T = \rho^2 v^2/2\chi + \ln(2\pi\chi)/2 \qquad (22)$$

where χ is the mean square fluctuation in the number of solvent molecules in a region with volume v and ρ is the number density of the solvent molecules. In this theory the importance of the density is clear, while the effect of hydrogen bonds enters *via* the width of the distribution. In our earlier work[7] on hard spheres in these model liquids at 300 K we found that the Gaussian approximation for the probability distribution breaks down in the wings, particularly for the modified water models. We are currently studying the temperature dependence of the distributions in all the model liquids and will report such calculations in a future publication.

Our results support many of the conclusions of earlier workers. Although in the Yu and Karplus approach[14] the chemical potentials of solutes and hence the solubilities of hydrophobic gases at a particular temperature are determined purely by solute–solvent terms, their temperature dependence and the entropy and enthalpy of solvation are strongly affected by the solvent reorganisation enthalpy which is abnormally low in SPC/E water. Thus at a given temperature we believe that the high number density and local packing in the liquid are the principal determining factors, but when the temperature dependence is considered one can associate the abnormal behaviour of water with its abnormally low solvent reorganisation enthalpy due to its three dimensional network structure, which is also manifest in the small value of its coefficient of thermal expansion.

Acknowledgements

PGD, PJR and THG gratefully acknowledge the support of this research by the U. S. National Science Foundation (CHE-0908265; CHE-0910615;CHE-0535616). PJR also acknowledges the generous support of the R. A. Welch Foundation (F-0019).

References

1 H. S. Ashbaugh and L. R. Pratt, *Rev. Mod. Phys.*, 2006, **78**, 159.
2 B. Ben-Naim, *Hydrophobic Interactions*, Plenum, New York, 1980.

3 D. Chandler, *Nature*, 2005, **437**, 640.
4 T. Lazaridis, *Acc. Chem. Res.*, 2001, **34**, 931.
5 D. L. Bergman and R. M. Lynden-Bell, *Mol. Phys.*, 2001, **99**, 1011.
6 R. M. Lynden-Bell and P. G. Debenedetti, *J. Phys. Chem. B*, 2005, **109**, 6527.
7 R. M. Lynden-Bell and T. Head-Gordon, *Mol. Phys.*, 2006, **104**, 3593.
8 T. Head-Gordon and R. M. Lynden-Bell, *J. Chem. Phys.*, 2008, **128**, 104506.
9 S. Chaterjee, P. G. Debenedetti, F. H. Stillinger and R. M. Lynden-Bell, *J. Chem. Phys.*, 2008, **128**, 124511.
10 J. Alejandre and R. M. Lynden-Bell, *Mol. Phys.*, 2007, **105**, 3029.
11 R. M. Lynden-Bell, *J. Phys.: Condens. Matter*, 2010, **22**, 284107.
12 B. Lee, *Biophys. Chem.*, 1994, **51**, 271.
13 K. P. Murthy, P. L. Privalov and S. J. Gill, *Science*, 1990, **247**, 559.
14 H. A. Yu and M. Karplus, *J. Chem. Phys.*, 1988, **89**, 2366.
15 B. Guillot and Y. Guissani, *J. Chem. Phys.*, 1993, **99**, 8075.
16 H. J. C. Berendsen, J. R. Grigera and T. P. Straatsma, *J. Phys. Chem.*, 1987, **91**, 6269.
17 H. Reiss, H. L. Frisch and J. L. Lebowitz, *J. Chem. Phys.*, 1959, **31**, 369.
18 F. H. Stillinger, *J. Solution Chem.*, 1973, **2**, 141.
19 K. Lum, D. Chandler and J. D. Weeks, *J. Phys. Chem. B*, 1999, **103**, 4570.
20 S. Garde, G. Hummer, A. E. Garcia, M. E. Paulitis and L. R. Pratt, *Phys. Rev. Lett.*, 1996, **77**, 4966.
21 S. Rajamani, T. M. Truskett and S. Garde, *Proc. Natl. Acad. Sci. U. S. A.*, 2005, **102**, 9475.
22 D. Ben-Amotz, F. Rainery and G. Stell, *J. Phys. Chem. B*, 2005, **109**, 6866.
23 G. Hummer, L. R. Pratt, A. E. Gárcia, A. Pohorille and L. R. Pratt, *Proc. Natl. Acad. Sci. U. S. A.*, 1996, **93**, 8951.
24 S. Sarupria and S. Garde, *Phys. Rev. Lett.*, 2009, **103**, 037803.
25 A. Ben-Naim, *Molecular Theory of Solutions*, Oxford University Press, Oxford, 2006.
26 B. Widom, *J. Chem. Phys.*, 1963, **39**, 2808.
27 M. P. Allen and D. J. Tildesley, *Computer Simulation of Liquids*, Clarendon Press, Oxford, 1989.
28 D. Frenkel and B. Smit, *Understanding Molecular Simulation: from Algorithms to Applications*, Academic Press Inc., San Diego, 2nd edn, 2002.
29 N. F. A. van der Vegt and W. F. van Gunsteren, *J. Phys. Chem. B*, 2004, **108**, 1056.
30 N. F. A. van der Vegt, D. Trzesniak, B. Kasumaj and W. F. van Gunsteren, *ChemPhysChem*, 2004, **5**, 144.
31 T. Lazaridis, *J. Phys. Chem.*, 1998, **102**, 3531.
32 T. Lazaridis, *J. Phys. Chem.*, 1998, **102**, 3542.
33 T. Lazaridis, *J. Phys.Chem.*, 2000, **104**, 4964.
34 J. R. Errington and P. G. Debenedetti, *Nature*, 2001, **409**, 318.
35 W. Smith and T. R. Forester, *The DL_POLY manual*, Daresbury Laboratory, 1996, http://www.cse.scitech.ac.uk/ccg/software/DL_POLY/index.shtml.
36 H. S. Ashbaugh, N. J. Collett, H. W. Hatch and J. A. Staton, *J. Chem. Phys.*, 2010, **132**, 124504.
37 S. Garde, A. E. Garcia, L. R. Pratt and G. Hummer, *Biophys. Chem.*, 1999, **78**, 21.
38 D. M. Huang and D. Chandler, *J. Phys. Chem. B*, 2002, **106**, 2047.
39 D. Ben-Amotz, *J. Chem. Phys.*, 2005, **123**, 184504.
40 G. Graziano, *J. Phys. Chem. B*, 2006, **110**, 11421.